Computers and Concrete, *Vol. 23, No. 3 (2019) 217-233*
DOI: https://doi.org/10.12989/cac.2019.23.3.217

Numerical investigation on punching shear of RC slabs exposed to fire

Hamed Sadaghian[a] and Masood Farzam*

Faculty of Civil Engineering, University of Tabriz, Tabriz, Iran

(Received September 12, 2018, Revised February 25, 2019, Accepted March 13, 2019)

Abstract. This paper describes the numerical modelling of an interior slab-column connection to investigate the punching shear resistance of reinforced concrete (RC) slabs under fire conditions. Parameters of the study were the fire direction, flexural reinforcement ratio, load levels, shear reinforcement and compressive strength of concrete. Moreover, the efficiency of the insulating material, gypsum, in reducing the heat transferred to the slab was assessed. Validation studies were conducted comparing the simulation results to experiments from the literature and common codes of practice. Temperature dependencies of both concrete and reinforcing steel bars were considered in thermo-mechanical analyses. Results showed that there is a slight difference in temperature endurance of various models with respect to concrete with different compressive strengths. It was also concluded that compared to a slab without gypsum, 10-mm and 20-mm thick gypsum reduce the maximum heat transferred to the slab by 45.8% and 70%, respectively. Finally, it was observed that increasing the flexural reinforcement ratio changes the failure mode from flexural punching to brittle punching in most cases.

Keywords: punching shear; fire; RC slab; temperature-dependent properties

1. Introduction

With the advancements in technology, there have been significant improvements in cementitious materials like concrete. Different types of concrete have emerged, the behaviour of which has been investigated under various conditions (Aslani *et al*. 2014a, 2015a). Nonetheless, the behaviour of concrete at elevated temperature is relatively unknown and with the global rise in temperature and consequently the number of accidental fires, the need to study the effect of fire is strongly felt.

During recent years, fire incidents have caused significant human and financial losses. According to Wijayasinghe (2011), in 2007, an aggregate of 42,753 fire incidents were recorded in several provinces of Canada with a substantial property damage of 1.5 billion dollars. According to the International Association of Fire and Rescue Services (2015), in 2013, 40% of fire accidents around the world were structural fires. Therefore, the fire phenomenon should be thoroughly studied.

Shear failures are not common in ordinary structures (Bamonte *et al*. 2009); nevertheless, the case is different for flat-plate structures. Punching shear in flat slabs is a major concern and despite numerous studies in recent decades (Wosatko *et al*. 2006, Kotsovos and Kotsovos 2010, Kotsovos 2014, Bompa and Onet 2016, Gosav *et al*. 2016, Farzam *et al*. 2017) which have shown its catastrophic consequences, there is scope for further research in this field.

Due to its brittle nature, progressive collapses may ensue from localized punching as the load is transferred to adjacent columns. Brittle punching occurs when concrete fails prior to the yielding of flexural reinforcements and flexural punching, which is a transition state between the brittle punching and flexural yielding, occurs when some of the rebars yield prior to the failure of the concrete and specimen fails before the formation of the flexural mechanism. In the case of fire, the issue becomes even more complex as the degradation of the material properties and increased internal forces due to thermal curvatures can cause the premature collapse of the structure.

This study presents a numerical modelling concerning the primary variables governing the punching shear strength of RC slabs under fire conditions. The effect of an insulating material, namely gypsum, with different thicknesses is also investigated. Concrete spalling under fire conditions is not considered in this study.

2. Research significance

There are numerous research in the literature regarding different issues in concrete structural members in the case of fire (Chung *et al*. 2006, Ibrahimbegovic *et al*. 2010, Hwang *et al*. 2013, Ožbolt *et al*. 2014, Hwang and Kwak 2015, Džolev *et al*. 2018); constitutive models have also been developed which have good correlation with experimental results (Aslani and Samali 2014b, 2015b). However, experimental data and numerical analyses on punching shear strength of RC slabs under fire conditions are very limited. To this end, a series of numerical analyses have been carried out to investigate the effect of influential parameters on punching resistance of RC slabs under fire conditions.

*Corresponding author, Assistant Professor
E-mail: mafarzam@tabrizu.ac.ir
[a]Graduate Student
E-mail: sadaghian.hamed@gmail.com

http://www.techno-press.org/?journal=cac&subpage=8
ISSN: 1598-8198 (Print), 1598-818X (Online)

Additionally, research on punching shear of slabs under fire conditions has been mostly conducted on concrete slabs with siliceous aggregates and no shear reinforcement. This study considers temperature-dependent material properties of calcareous concrete as well as shear reinforcement.

3. Existing data on punching shear under fire conditions

The collapse of the roof of a parking garage in Gretzenbach, Switzerland (Fernández Ruiz *et al*. 2010) raised concerns over the punching shear behaviour of flat slabs in fire. Fire resistance of a multi-bay RC structure consisting of flat slabs supported by perimeter beams was numerically studied by Moss *et al*. (2008). Slabs of all the nine bays in the lowest story were subjected to fire scenarios with and without decay phase. The analyses investigated several parameters with no specific discussion of the punching shear. Also, it is noteworthy that they completely neglected the tensile strength of concrete in their numerical models. George and Tiang (2012) carried out nonlinear finite element analyses on a four-story multi-bay office building with slab dimensions of 1830×1830×152 mm^3 without shear reinforcement; the primary focus was on the slab, with the assumption that no flexural or bending failure occurs in the slab. They neglected the evaporation of free water and the mass density of concrete was taken constant. They concluded that column restrains the thermally induced rotation of the slab with a consequential result of top rebar yielding and severe moment redistribution. Bamonte *et al*. (2012) extended the critical shear crack theory to the case of high temperatures and/or fire. The primary assumption of the theory that "*a diagonal shear crack forms at early loading stages and influences the behaviour of the whole slab-column assembly"* was valid. They reported a good correlation between the proposed method and the experimental data (Kordina 1997). However, they clearly outlined the significance of conducting further experiments and studies to (a) consider the thermally-restrained support conditions and (b) to adapt existing code requirements to consider punching shear during fire. Bamonte and Felicetti (2009), Annerel *et al*. (2013) studied the impacts of a real fire model on a slab-column assembly of a parking structure. Their study showed that heating non-uniform spans remarkably increases the shear force in the slab-column connection with a consequential result of a 50% increase in the axial load of the column. It is worth mentioning that Bamonte and Felicetti (2009) neglected concrete cracking and rebar yielding.

Numerous factors affecting the punching shear resistance of RC slabs under fire conditions including the direction of fire, concrete cover, flexural reinforcement ratio, support conditions, duration of fire, etc. have been investigated by researchers. In following, some of the available research in this regard is discussed:

Bamonte *et al*. (2009) argued that the redistribution of internal forces ensuing from indirect actions under fire conditions can cause the punching shear to increase by 10%-30%. Fire direction which could also influence the redistribution of internal forces was investigated by Liao *et al*. (2013); fire endurance of slabs varied significantly with respect to different fire directions. Punching shear for the fire loading on the tension side occurred after 3-5 hours while no failure was observed for the fire loading on the compression side even after 8 hours.

The influence of real-case fire scenarios on punching shear resistance of RC slabs was investigated by Annerel and Taerwe to (2013) to study the effect of stirrups. For the configuration tested, a minimal contribution of stirrups to the punching shear was reported. It was also hypothesized that for the fire safety of buildings, the load-bearing capacity of slabs may be estimated without stirrups. Whether this is a credible claim or not is debatable as the authors clearly suggested further research in this regard.

Salem *et al*. (2012) exposed 14 one-third scale specimens (2 at ambient temperatures) to fire conditions on their tension side. Variables of the study were the concrete cover, fire duration, and the cooling method. Based on their findings, exposure of slabs to fire reduced the first cracking and the ultimate load capacities by 18.3% and 43%, respectively. Furthermore, concrete cover proved to be very effective in reducing the heat transferred to the concrete. Relatively poor performance was also reported for long-term (3 hours) fire subjection compared to short-term ones (1 hour), i.e., 14% reduction in punching shear strength. The observation that the increase in the flexural reinforcement ratio increases the punching shear capacity of RC slabs both at ambient and elevated temperatures was reported by Ghoreishi *et al*. (2015); the authors strongly recommended that the effect of flexural reinforcement ratio be included in Canadian Standard (CA) code provisions.

Smith *et al*. (2016) tested 15 series of slab-column connections in punching shear both at ambient and elevated temperatures. The slabs had dimensions of 1400×1400 mm^2 with varying thicknesses, i.e., 50 mm, 75 mm and 100 mm. The effect of different support conditions was also investigated; an unusual slab-column deflection away from the heated surface and in the direction of the loading was reported.

Review of the previous studies shows that all the authors have highlighted the catastrophic effects of fire on punching shear of RC slabs and the need to consider the influence of various factors. Studies showed that parameters such as the fire direction, flexural reinforcement ratio, concrete cover, fire duration and support conditions highly influence the punching resistance of RC slabs. Besides, it was highlighted that further studies are required to adapt code provisions to consider fire effects on the punching resistance of RC slabs.

In this study, the influence of fire direction, flexural reinforcement ratio, presence/non-presence of stirrups and compressive strength of concrete were studied. To consider the effect of concrete cover, instead of increasing the concrete cover, an insulating material, namely, gypsum was used in two different thicknesses.

4. Materials at elevated temperatures

4.1 Gypsum

Gypsum is one of the common fire insulating materials.

The challenging issue in the numerical modelling of these materials is the fact that temperature-dependent equations for these materials are limited or no unified models exist in the reported data (Wang 2012) to allow for the development of a consistent model. In this study, gypsum was chosen as the insulating material, first for its low thermal conductivity compared to concrete (0.24 W/m℃ versus 1.95 W/m℃) and second for the availability of its data (Wang 2012).

Gypsum ($CaSO_4.2H_2O$, calcium sulphate dehydrate) has about 3% (by weight) of free water and 21% (by weight) chemically-bound water; when exposed to elevated temperatures, a two-phase chemical reaction occurs as follows (Eqs. (1)-(2)) and the 21% free water evaporates (Wang 2012):

$$\mathrm{CaSO_4.2H_2O} + Q_1 \rightarrow \mathrm{CaSO_4.2H_2O} \tag{1}$$

$$\mathrm{CaSO_4}.\frac{1}{2}\mathrm{H_2O} + Q_2 \rightarrow \mathrm{CaSO_4} + \frac{1}{2}\mathrm{H_2O} \tag{2}$$

The first reaction occurs roughly at the same time with the loss of free water at about 80℃-120℃ where gypsum is decomposed to calcium sulphate hemihydrate and 75% of the chemically-bound moisture content is released. When the temperature is about 220℃ the remaining chemically-bound moisture content is also released (Wang 2012). The endothermic reaction, i.e., evaporation of water, requires a substantial amount of heat which in turn, delays the temperature increase in gypsum (Kontogeorgos *et al*. 2015). This characteristic of gypsum along with its low thermal conductivity makes it a cheap fire insulating material to be used in residential and commercial buildings.

4.2 Concrete

Concrete experiences different phase changes as the temperature increases which affect its microstructure. According to Hertz (2005), up to temperatures of 100℃-150℃ only the free water present in the pores of concrete evaporates and therefore mechanical properties of concrete remain almost unchanged. Thereafter, the chemically-bound water in calcium silicate hydrates (CSH) in the cement matrix starts being released with the temperature increasing to around 270℃ (Hertz 1980). This phase is characterized by the drop of compressive strength by 10%-15% which is reversible provided that the temperature doesn't increase beyond this level and normal cooling conditions occur instead of thermal shocks or water cooling (Hertz 2005). After this phase and between the 400℃-600℃ temperature range, calcium hydroxide crystal present in the cement matrix starts to decompose to calcium oxide and reaches its highest intensity around 535℃ (Hermathy 1970). In this phase not only decomposition of hydroxide crystals has detrimental effects on concrete strength but also reaction of calcium oxide with the water vapour present in the air creates calcium hydroxide which is 44% larger in volume than that of calcium oxide (Petzold and Röhrs 1970) and widens the previously-formed micro cracks with a consequential result of further deterioration in the mechanical properties of concrete. Going beyond 600℃, further micro cracking and deterioration of mechanical properties, ensuing from further decomposition of calcium compound occur with their peak at 710℃. According to Hermathy (1970), at about 500℃, 70% of the dehydration is complete and at 850℃, CSH is completely depleted.

Regarding structural parameters, numerous relationships have been given by researchers and codes which can be found in Appendix A (Tables A1-A5). Based on the proposed relationships for compressive strength, tensile strength and modulus of elasticity, it can be observed that all the three parameters deteriorate with the rise in temperature. Aggregate type is found to highly affect the compressive strength of concrete; mixes with lower cement contents maintain their strength better than those with higher cement ratios. The reason why these parameters affect the deterioration of concrete has been briefly discussed in the foregoing paragraph. Moreover, it's been shown that modulus of elasticity of concrete is mostly affected by the same parameters as its compressive strength (Malhorta 1982).

Naus (2010) investigated the data from numerous researchers and concluded that the effect of aggregate type and concrete mix proportions on the tensile strength of concrete is significant while heating rate had a minimal effect. Furthermore, based on the experimental studies of Carette *et al*. (1982) the importance of considering the duration of fire exposure was highlighted. Finally it's been reported that the rate of tensile strength deterioration is independent of the concrete strength and aside from the risk of spalling, high-strength concrete behaves in the same manner as the normal-strength concrete (Phan 1996).

Despite these findings, temperature is the only variable considered by the researchers as can be seen in appendix A and the effect of the above-mentioned parameters is neglected.

4.3 Steel

The absence of a distinct yielding plateau and occurrence of strain-hardening behaviour starting at 100℃ has been reported by numerous researchers such as Custer and Meacham (2000). The behaviour of steel during a fire is better comprehended than concrete and according to Fletcher *et al*. (2007), Hertz (2003), the most notable processes in steel during a fire is as below:

-At temperature range between 200℃ and 300℃, steel rebars with low carbon content take a blue colour with an increase in strength. The increase of strength causes the steel to lose its ductility and become more brittle. It is recommended that to avoid this phenomenon, the steel be kept protected from temperatures higher than 250℃ - 300℃. After 300℃, modulus of elasticity decreases with the rise in temperature while the yield stress remains almost the same up to 400℃.

-The thermal expansions of concrete and steel are relatively the same up to 400℃. Beyond this temperature, thermal expansion of steel becomes significantly larger than that of concrete with a consequential result of increased internal stresses and the high risk of bond failure.

-At 700℃, design load-bearing capacity of steel reduces to about 20% of its initial value.

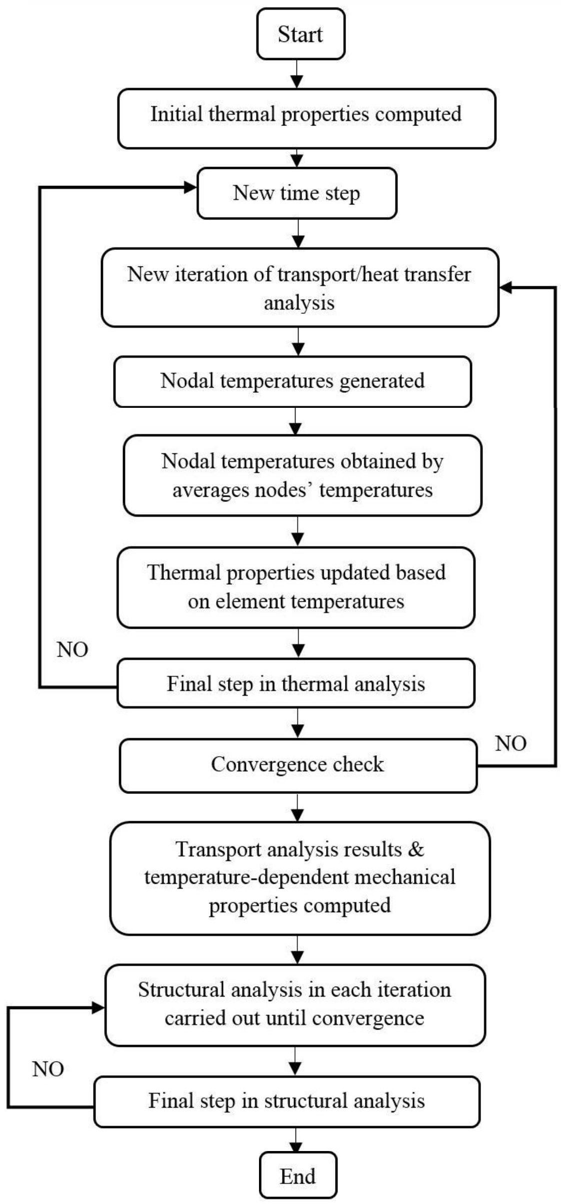

Fig. 1 Flowchart of the coupled thermo-mechanical analysis

5. Thermo-mechanical analysis

5.1 Introduction

ATENA (2016) is an advanced engineering tool capable of simulating the real behaviour of concrete under various conditions. Its modelling capabilities have been validated against test results both in terms of thermal and structural fire behaviour (Aslani *et al*. 2015c, Firmo *et al*. 2015, Jadooe *et al*. 2017) and static problems including punching and other shear-related problems (Farzam *et al*. 2010, Cervenka 2013, Farzam *et al*. 2017).

The flowchart of the coupled thermo-mechanical analysis is shown in Fig. 1. As it can be seen, the coupled thermal and structural analyses are time-stepped. The mechanism consists of two steps. At first, the created model is exposed to a pre-defined temperature-time regime along certain surfaces. The procedure is continued by simulating conductive-radiative phenomena which occur from free surfaces and boundaries of the model. Due to the incremental nature of the problem, heat transfer equations are solved based on an iterative algorithm while taking into account the temperature-dependent thermal properties.

The heat transfer analysis applies the temperature to all nodes that create the finite element model. These temperatures are averaged and then converted to temperatures of finite elements. The second step of the analysis is a separate structural analysis where previously obtained results from the thermal analysis are imported at desired intervals to determine the behaviour of the structure based on temperature-dependent mechanical properties. This process is also iterative and is repeated during each time step. Material properties are updated at each time interval and temperature increment. This procedure is capable of capturing the nonlinear response of structures subjected both to external loads and temperature fields and/or fire.

5.2 Materials and solution methods

The concrete model that was used in ATENA (2016) was *CC3DNonLinCementitous2*, which is based on the fracture-plastic model. Eight-node 3-D solid brick elements were used to model the concrete, loading plate and steel supports. Rebars were modelled as bi-linear strain-hardening 1-D truss elements embedded in concrete. For concrete, the temperature-dependent material properties including thermal conductivity (k_c, (W/m℃)), specific heat capacity (ρc), density (ρ), compressive strength (f_c') and thermal expansion strain (ε_{th}) were based on Eurocode 2 (EC2) (BS EN1992-1-2:2004). For the modulus of elasticity (E_c), critical compressive displacement (W_d), plastic strain at peak compressive stress (ε_{cp}), f_c' and ε_{th} coefficients were considered which were multiplied to the initial value of the parameters at normal temperatures as shown in Figs. 2(a)-(e). It should be noted that the model proposed by EC2 (BS EN1992-1-2:2004) for tension is incapable of simulating the real behaviour of concrete in tension since it loses its strength at 600℃. To remedy this problem, in this study, in all the subsequent sections, the model proposed by Dwaikat and Kodur (2009) is used for the tensile strength of concrete. This model is favourable for finite element computer programs as the numerical instabilities that may result from analysing the behaviour of concrete with absolutely no tensile strength are avoided. The formula is shown in Eq. (3)

$$f_{tT}' = \begin{cases} f_t' , & T < 100℃ \\ f_t'(\dfrac{600-T}{500}), & 100℃ \le T < 550℃ \\ f_t'(\dfrac{1200-T}{6500}) & 550℃ \le T < 1200℃ \\ 0 & T \ge 1200℃ \end{cases} \tag{3}$$

where f_{tT}' and f_t' are tensile strengths of concrete at elevated and normal temperatures, respectively and T is the temperature of concrete.

With regard to rebars, the stress-strain diagram is scaled based on the maximum temperature reached at each rebar element based on EC2 (BS EN1992-1-2:2004) formulas.

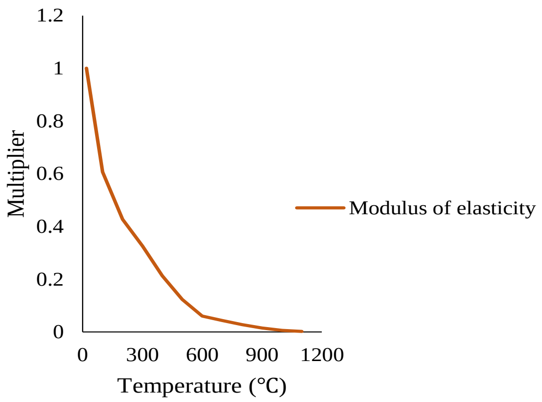

(a) Modulus of elasticity

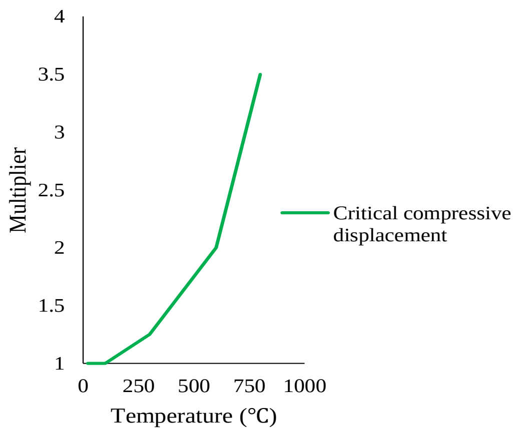

(b) Critical compressive displacement

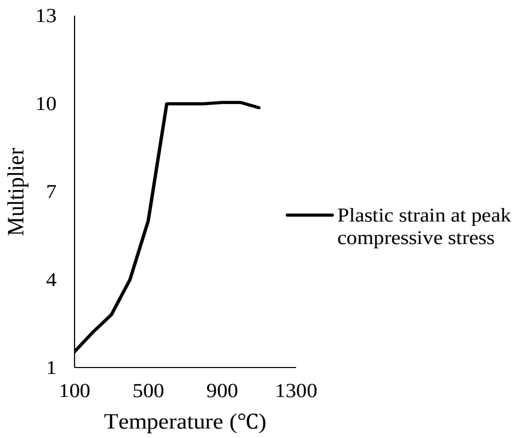

(c) Plastic strain at peak compressive stress

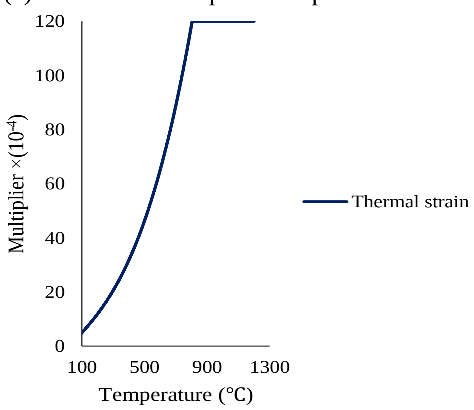

(d) Thermal strain of concrete

Fig. 2 Temperature dependence of concrete properties

"Fire boundary for surface" boundary condition was used in ATENA (2016)-GID (2015) interface to apply the fire load to the surface of the slab.

Concerning the non-linear iterative solvers, Newton-Raphson method with line search function was used to carry-out the analyses; the Newton-Raphson method is efficient in cases where the load values must be exactly met. It should be used in case of temperature loading (ATENA, 2016). Four solution errors serve to check the following criteria: (1) displacement increment, (2) normalized residual force, (3) absolute residual force, (4) energy dissipated. The relative value for the first three criteria was set to 0.01, while the relative value for criterion four was set to 0.0001; Conditional break criteria were set to stop the computation if an error exceeded the tolerance multiplied by the factor during the iterations (multiplier equal to 10,000 for the first three criteria and 100,000 for the fourth criteria) or at the end of an analysis step (multiplier equal to 10 for the first three criteria and 100 for the fourth criteria).

6. Validation studies

6.1 Mechanical response of a slab

The slab-column assembly (specimen SB1) tested by Adetifa and Polak (2005) and used by Genikomsou and Polak (2015) was chosen to validate the numerical modelling of the punching shear. Material properties of concrete are shown in Table 1. The given slab was of dimensions 1800×1800×120 mm^3 simply supported on 40 mm-wide, 25 mm-thick steel plates along the edges. In the numerical model, the bottom face of the steel support was placed on a line support at its centre which reasonably simulated hinged supports; the height of the column extending from the top and bottom faces of the slab was 150 mm; Φ10 rebars were used at 90 and 100 mm centres for the top and bottom layers in the tension mat. Similarly, Φ10 rebars were used at 200 mm centres for the top and bottom layers of the compression mat. Concrete cover was 20 mm in both tension and compression mats and the

Table 1 Properties of simulated materials (Genikomsou and Polak 2015)

Property	Concrete	Steel
$\boldsymbol{f'_c}$(MPa)	44	---
$\boldsymbol{f'_t}$ (MPa)	2.2	---
$\boldsymbol{E_c}$ (MPa)	36,483	---
$\boldsymbol{G_F}$ (N/mm)	0.082	---
$\boldsymbol{\sigma_Y}$ (MPa)	---	455
$\boldsymbol{\varepsilon_Y}$	---	0.0023
$\boldsymbol{\sigma_{Frac.}}$ (MPa)	---	650
$\boldsymbol{\varepsilon_{Frac.}}$	---	0.25

Note: G_F: Fracture energy of concrete; σ_Y: Yield strength of rebars; ε_y: Yield strain of rebards; $\sigma_{Frac.}$: Fracture stress of rebars; $\varepsilon_{Frac.}$: Fracture stress of rebars

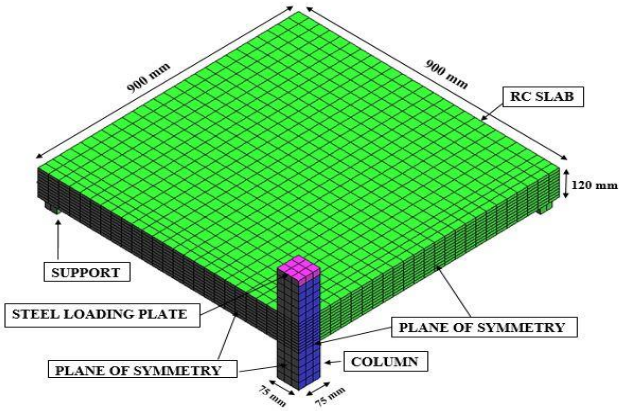

(a) Numerical model

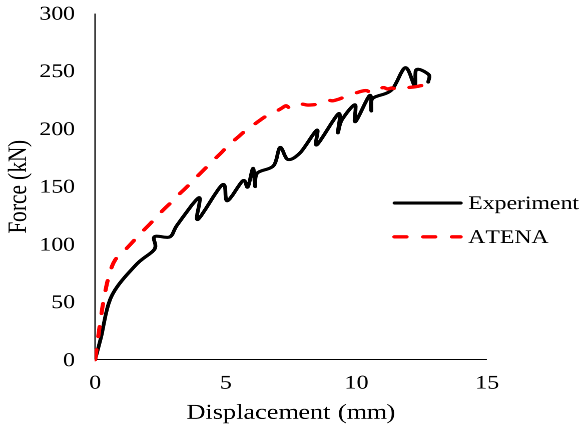

(b) Comparison of numerical and experimental results (Genikomsou and Polak 2015)

Fig. 3 Numerical model and comparison of results

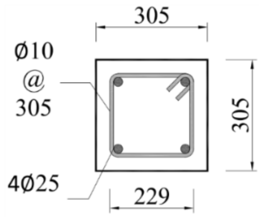

Fig. 4 Cross-section of the experimental model (Elmohandes 2013, Elmohandes and Vecchio 2016)

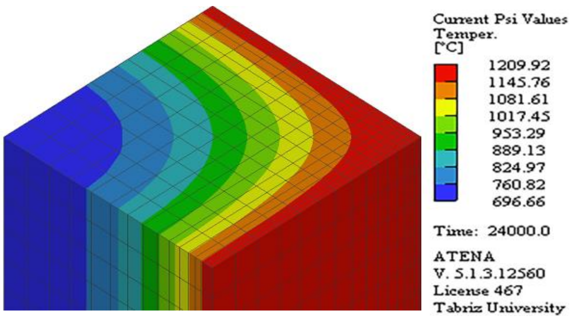

(a) Thermal analysis

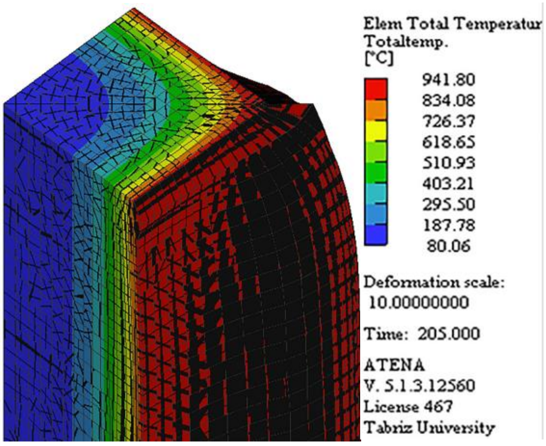

(b) Deformed shape and temperature distribution in the thermo-mechanical analysis

Fig. 5 Temperature distribution and deformed shape in the column

column had a square cross-section of 150×150 mm reinforced with four 20 mm rebars enclosed by four 8 mm ties. Taking advantage of symmetry, one-quarter of the slab-column assembly was modelled. Displacement and the corresponding force values were monitored at the centre of the column section. The load was applied in a displacement-controlled manner until failure. The numerical model is shown in Fig. 3(a). The load-displacement curve (Fig. 3(b)) which indicates brittle punching is in agreement with the findings of Genikomsou and Polak (2015).

6.2 Thermal and mechanical response of a RC element

In order to validate the thermal capabilities of ATENA (2016), a thorough experimental data is required to ensure the methodology implemented in the subsequent sections. Moreover, since the primary focus of this section is the evaluation of thermal capabilities of ATENA (2016) and not the type of the structural element, a study is chosen from the literature which has adequate and detailed experimental data. To this end, both the thermal and static results of a column tested by Elmohandes (2013) and Elmohandes and Vecchio (2016) are validated in this section. Material properties are according to EC2 (BS EN1992-1-2:2004) and ASCE (1993).

6.3 Discussion of results

Table 1 summarises the numerical and experimental results from validation. As it can be seen in Table 1, ATENA (2016) yields a very good estimation of "*e*". It should be noted that the data provided in Fig. 6(d) were limited to 118 minutes for the numerical simulation and 152 minutes for the experimental results because excessive spalling was reported by Elmohandes (2013) and Elmohandes and Vecchio (2016) for the descending part of the graph which is not within the scope of this study.

ASCE (1993) does not take into account the effect of moisture content in specific heat capacity which is in contradiction to reality. ASCE (1993) correlates better with the experimental results in shallow depths of the concrete section close to the heated surface where water evaporates and virtually no water is present; on the other hand, in inner depths of the column section and/or when the moisture

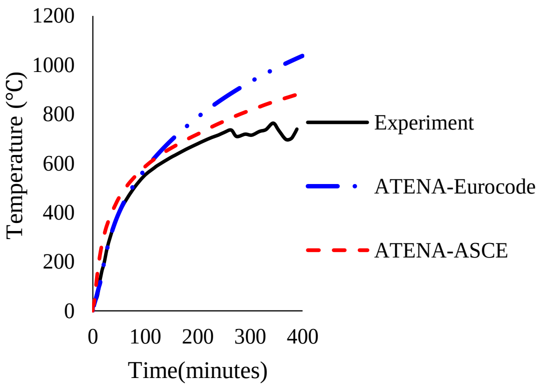

(a) Temperature change at a depth of 25 mm

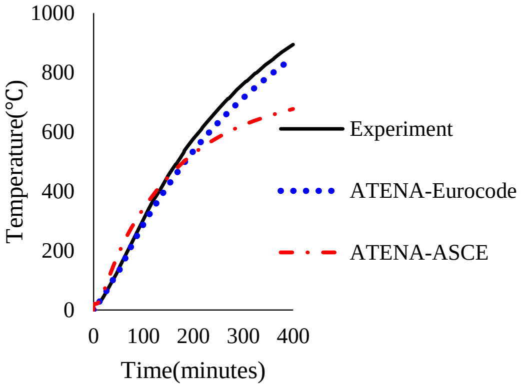

(b) Temperature change at a depth of 62.5 mm

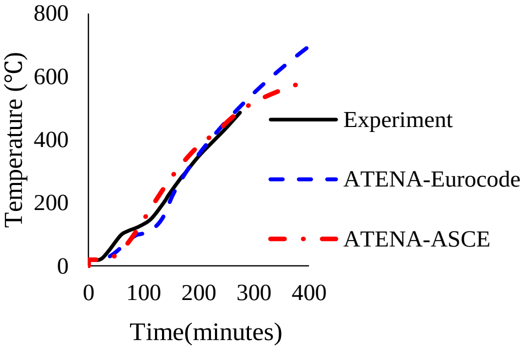

(c) Temperature change at a depth of 152.5 mm

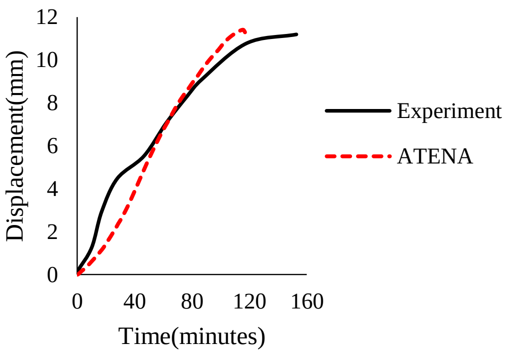

(d) Static results

Fig. 6 Experimental and numerical results for the column tested by Elmohandes and Vecchio (2016)

content is high, ASCE (1993) fails to provide good estimations of real-case scenarios. EC2 (BS EN1992-1-2:2004), in contrast to ASCE (1993), provides better estimations when moisture content is high. Based on the results obtained from the validation (Table 2), it can be concluded that ATENA (2016) is capable of simulating the real behaviour of concrete reasonably and EC2 (BS EN1992-1-2:2004) provides the nearest estimation to reality which will be used in the subsequent sections.

Table 2 Experimental and analytical results by Elmohandes and Vecchio (2016) and ATENA (2016)

Specimen	Experimental results		ASCE		EC2		ATENA	
	e (mm)	*t* (min)	*e* (mm)	*t* (min)	*e* (mm)	*t* (min)	*e* (mm)	*t* (min)
Column	11.10	510	12.50	517	11.06	598	11.29	118

Note: *e*: Maximum expansion reached from the start of the fire; *t*: Duration from the start of the fire to failure

7. Finite element model of a slab subjected to fire

Specimen SB1 tested by Adetifa-Polak (2005) and used by Genikomsou and Polak (2015) was used as a baseline to ensure punching shear failure at ambient temperatures. Calcareous aggregates, were used for concrete. Calcareous aggregates are more stable than other types of aggregates when exposed to elevated temperatures; their thermal expansion coefficient is smaller than that of other aggregates and is close to the thermal expansion coefficient of cement matrix (Cather 2003). Furthermore, calcareous aggregates perform better than siliceous aggregates from a thermal expansion point of view which is also corroborated by ACI 216.1-14 (2014) and BS 8110-2:1985 (1985). Because the coupled thermal and structural analysis involves two distinctive steps, two models were required to be analysed. First, the thermal model is discussed and then the structural model.

7.1 Fire applied from top

Temperature-dependent material properties that governed the thermal analysis were based on EC2 (BS EN1992-1-2:2004). Other properties concerning thermal analyses included the convective heat transfer and emissivity for which 25 W/m^{2}C and 0.7 values were used, respectively. ISO834-1 (1999) fire curve was used for the ascending part for three hours followed by a 2-hour cooling phase. It should be noted that the primary objective of this study is to investigate the behaviour of the specimen under fire conditions and the 2-hour cooling phase is merely presented for comparative purposes in terms of the maximum temperature transferred to the slab in cases with and without gypsum in the thermal analyses only. Besides, since the specimen fails prior to reaching the descending branch of the temperature-time curve, definition of material properties corresponding to the cooling phase was not required in the mechanical analyses. Temperature was monitored in three locations of the slab depth, top face, middle and bottom face. Furthermore, Fig. 7 shows the distribution of heat in the slab after 3 and 5 hours and the

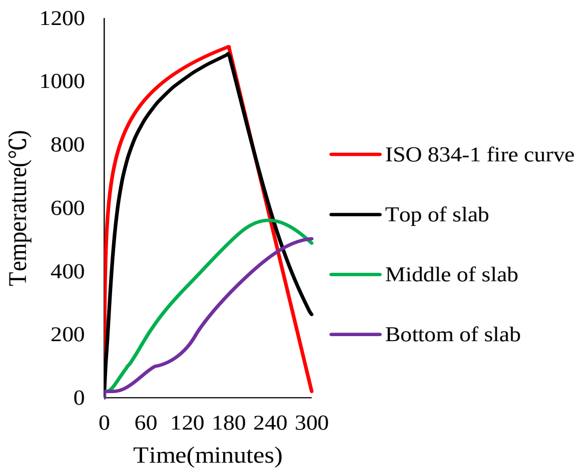

Fig. 7 Temperature-time curves in different depths of slab after 5 hours (fire is applied from top)

temperature-time curve, respectively.

The slight difference between the ISO 834-1 (1999) fire curve and the monitoring on top of the slab can be attributed to the convection phenomenon between the air and the slab surface. This difference is noticeable in the descending branch owing to the fact that inner parts of the slab prevent the top surface of the slab from cooling down fast.

7.2 Fire applied from bottom

In this case, the loading conditions and geometry of the specimen were similar to the previous section except for the fire direction which was applied from the bottom face. Similar trends to the case when fire was applied from the top face were obtained and therefore the results are not shown for brevity.

7.3 Fire applied from the bottom to a slab insulated with gypsum

Two thicknesses of gypsum (i.e., 10-mm and 20-mm) were used to assess the insulating performance of gypsum. Properties of gypsum are based on the work by Rahmanian and Wang (2012). Temperature- dependent thermal properties of gypsum are shown in Figs. 8(a)-(c). Figs. 8(a)-(b) show the temperature evolution in the slab in presence of 10-mm and 20-mm thick gypsum after 5 hours, respectively. As it can be seen in Figs. 7 and 9 for a slab without gypsum, the maximum temperature reached is 1086.6℃, which decreases by 45.8% and 70% and reaches to 588.7℃ and 327.4℃ for the slab with 10-mm and 20-mm gypsum, respectively.

7.4 Structural analysis

In following, sensitivity analyses are carried out based on the work by Genikomsou and Polak (2015). Due to symmetry, only one-quarter of the specimen was modelled. 0.1 to 0.9 multiples of the pure gravity failure load (PGFL) (i.e., no fire application) were applied at the centre of the

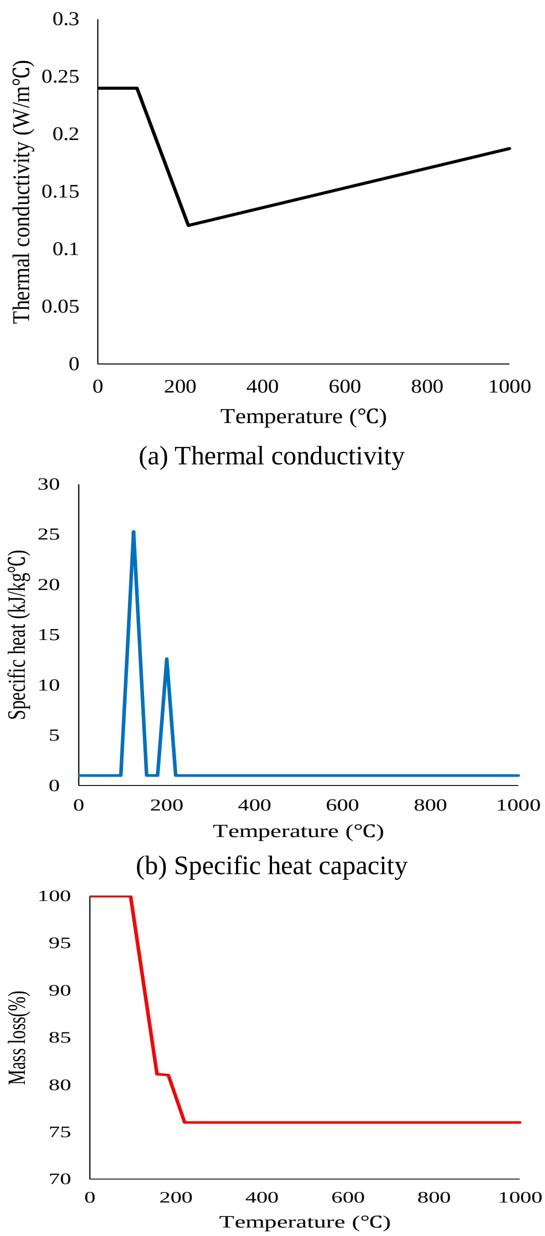

(a) Thermal conductivity

(b) Specific heat capacity

(c) Mass loss (%)

Fig. 8 Temperature-dependent material properties of gypsum (Rahmanian and Wang 2012)

column fire in the first interval (different load levels can be used to simulate the load distribution that may occur in a slab exposed to fire (Bamonte *et al*. 2012) and play an important role in fire endurance (Kodur and Phan, 2007). In the second interval, the load value was kept constant while results from thermal analyses were imported. The variables were: flexural reinforcement ratio, load levels, compressive strength of the slab and shear reinforcement (investigating the effect of shear reinforcement was necessary because, among the 47 tested specimens in punching shear under fire conditions reviewed by Arna’ot *et al*. (2017), only six specimens included shear reinforcement in varying configurations and ratios). It should also be mentioned that the compressive strength of the column was increased to 60 MPa in all cases so that failure doesn’t

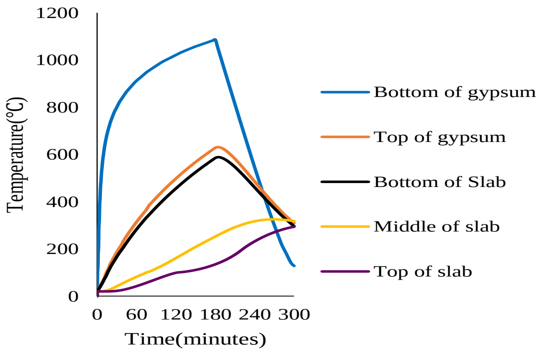

(a) 10-mm thick gypsum

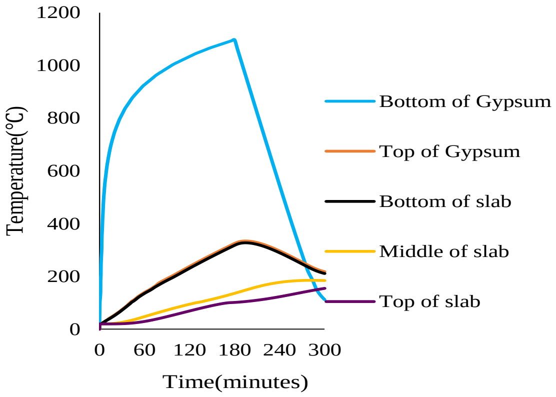

(b) 20-mm thick gypsum

Fig. 9 Evolution of temperature in slab in presence of gypsum after 5 hours

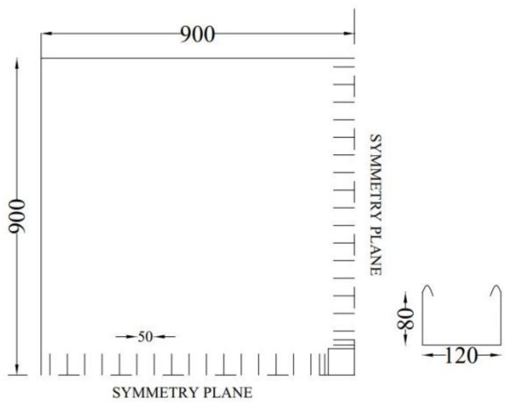

Fig. 10 Layout of the a quarter of the slab (dimensions are in mm)

occur in the column and cracks and failure mechanism become more distinct in the slab.

Displacement and force values were monitored at the centre of the column. Temperature was monitored at the top face of the slab. Moreover, Φ10 stirrups at 50 mm centres with a yield strength of 455 MPa were used as shear reinforcements in two orthogonal directions in their respective cases in subsequent sections (the layout is shown in Fig. 10).

7.5 Sensitivity analyses

Different cases were considered to investigate the influence of the above-mentioned variables as follows:

Case 1: No shear reinforcement in the slab (f_c'= 44 MPa), average rebar ratio, $\bar{\rho}$ = 0.85% (flexural rebar size, 8 mm) and fire application from the top face (PGFL is 165.28 kN). Results are shown in Figs. 11(a)-(b) and 12(a)-(b).

Case 2: Shear reinforcement in the slab (f_c'= 44 MPa), $\bar{\rho}$= 0.85% (flexural rebar size, 8 mm) and fire application from the top face (PGFL is 170.87 kN). Results are illustrated in Figs. 12(c)-(d).

Case 3: No shear reinforcement in the slab (f_c'= 44 MPa), $\bar{\rho}$ = 2.61% (flexural rebar size, 14 mm) and fire application from the top face (PGFL is 247.59 kN). Results are presented in Figs. 13(a)-(b).

Case 4: Shear reinforcement in the slab (f_c'= 44 MPa), $\bar{\rho}$ =2.61% (flexural rebar size, 14 mm) and fire application from the top face (PGFL is 343.11 kN). Results are presented in Figs. 13(c)-(d).

Case 5: No shear reinforcement in the slab (f_c'= 60 MPa), $\bar{\rho}$ = 2.61% (flexural rebar size, 14 mm) and fire application from the top face (PGFL is 288.17 kN), Aslani and Bastami (2011) model for f_c'. Results are shown in Figs. 14(a)-(b).

Concrete with compressive strength greater than 55 MPa is considered as high-strength concrete by ACI 363R-10 (2010). Since high-strength concrete loses its strength more rapidly than normal concrete (due to high heating rate and low permeability of high-strength concrete which results in pressure build-up in case of fire) a model for high-strength concrete proposed by Aslani and Bastami (2011) was used for temperature-dependent compressive strength of concrete (it should be noted that according to Kodur and Dwaikat (2008), the risk of spalling for concrete strengths of 70 MPa or lower is minimal). The relationship proposed by Aslani and Bastami (2011) is shown in Eq. (4)

$$f_{cT}' = \begin{cases} f_c'(1-10^{-2}-6\times10^{-4}T \le 1.0 & T \le 200℃ \\ \quad f_c'(1.0565-17\times10^{-4}T & \\ +5\times10^{-6}T^2-5\times10^{-9}T^3) & 100℃ < T \le 900℃ \\ 0 & T > 900℃ \end{cases} \tag{4}$$

Case 6: Shear reinforcement in the slab (f_c'= 60 MPa), $\bar{\rho}$= 2.61% (flexural rebar size, 14 mm) and fire application from the top face (PGFL is 343.11 kN). Aslani and Bastami (2011) model for f_c'. Results are shown in Fig. 14(c)-(d).

Case 7: Shear reinforcement in slab (f_c'= 60 MPa), $\bar{\rho}$= 2.61% (flexural rebar size, 14 mm) and fire application from the bottom face (PGFL is 343.11 kN). Aslani and Bastami (2011) model for f_c'. Results are shown in Fig. 15(a)-(b).

8. Results and discussions

In case 1, according to Fig. 12(a) which shows no ductile behaviour and the fact that rebars didn't yield, the failure mode of the specimen was brittle punching in ambient temperatures. Brittle punching was the failure mechanism up to 0.5×PGFL; the failure mechanism changed to flexural punching for greater load levels as the rebar yielding propagated from the column perimeter

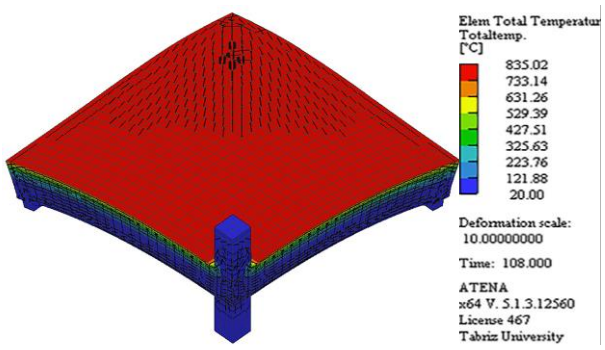

(a) 0.1×PGFL

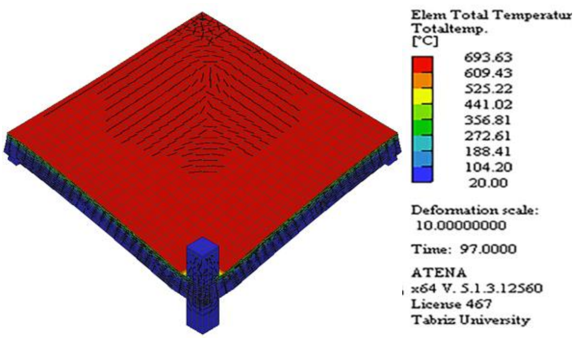

(b) 0.9×PGFL

Fig. 11 Temperature contour, deformed shape and crack pattern in case 1

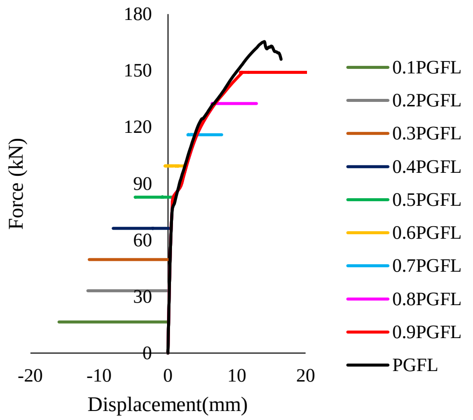

(a) Case 1

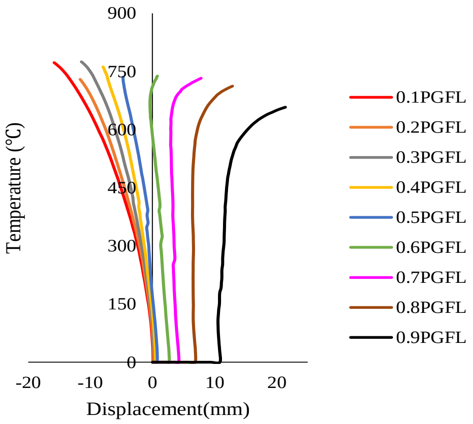

(b) Case 1

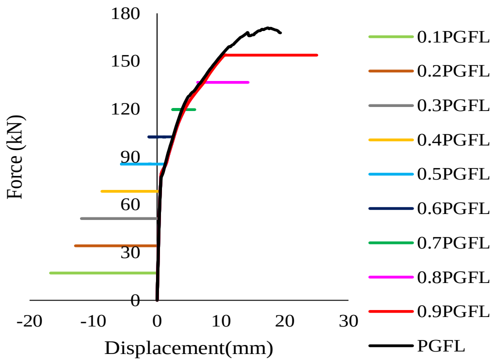

(c) Case 2

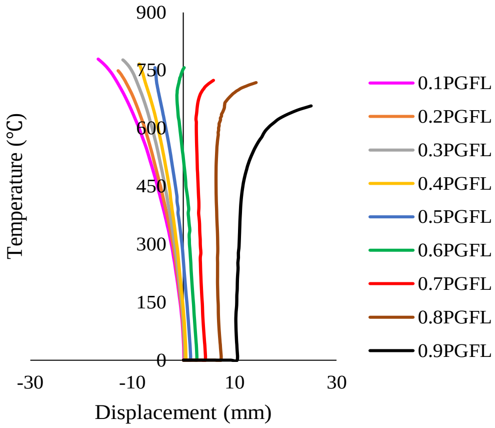

(d) Case 2

Fig. 12 Force-displacement and temperature-displacement curves

towards supports; however, this development was not significant enough to cause flexural yielding. No significant trend was observed for the overall fire endurance with respect to different load levels according to Fig. 12(b). However, in this case and all the subsequent cases, for load levels greater 0.7×PGFL, a slightly decreasing trend was observed. Additionally, for the foregoing load level, fire was unable to deflect the slab upwards, in contrast to lower load levels according to Fig. 11(a)-(b).

In case 2, which is similar to case 1 except that it has shear reinforcements, according to stress values in rebars and Fig. 12(c), the failure mode of the specimens was flexural punch in ambient temperatures. This was also valid for all the load levels in this case. Similar to the previous case, fire was unable to deflect the slab upwards, in contrast to lower load levels according to Fig. 12(d).

In case 3, increasing the flexural reinforcement ratio increased the load capacity both in ambient and elevated temperatures and the failure mode was brittle punching according to Fig. 13(a). A decreasing trend was observed for the temperature endurance for load levels greater than 0.7×PGFL according to Fig. 13(b).

With regard to case 4, the failure mode of the specimen was brittle punching both in ambient and elevated temperatures except for the 0.9×PGFL; as shown in Figs. 13(c)-(d) the deflection was in the direction of the gravity load in this load level. Comparisons of case 3 and 4 based on Figs. 13(a)-(b) and Figs. 13(c)-(d) for the same load value show that shear reinforcement have negligible contribution to the temperature sustained by the specimen. It can be seen that for an equal load value, displacement values corresponding to failure are almost the same.

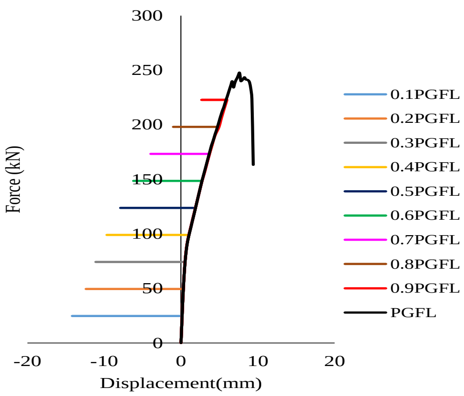

(a) Case 3

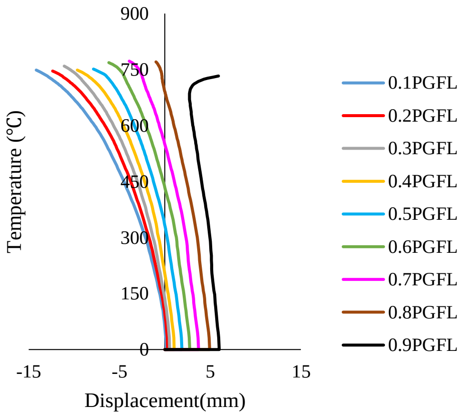

(b) Case 3

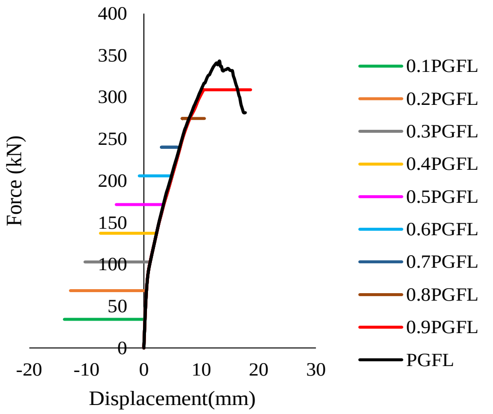

(c) Case 4

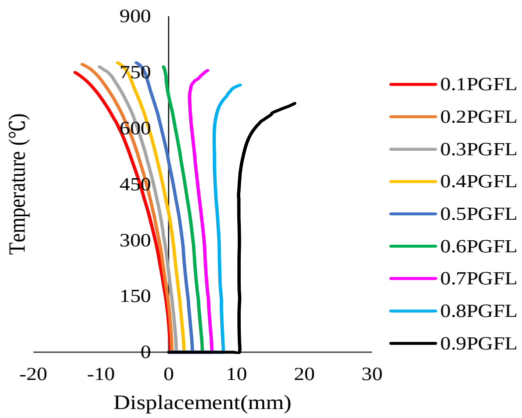

(d) Case 4

Fig. 13 Force-displacement and temperature-displacement curves

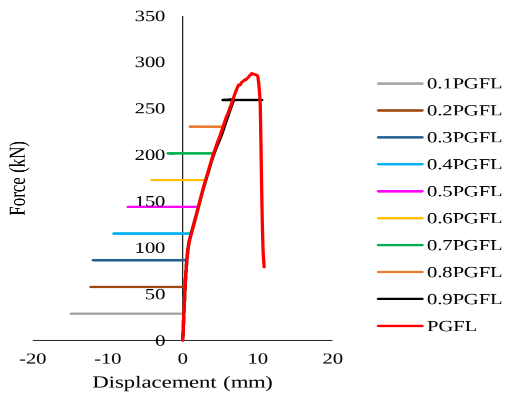

(a) Case 5

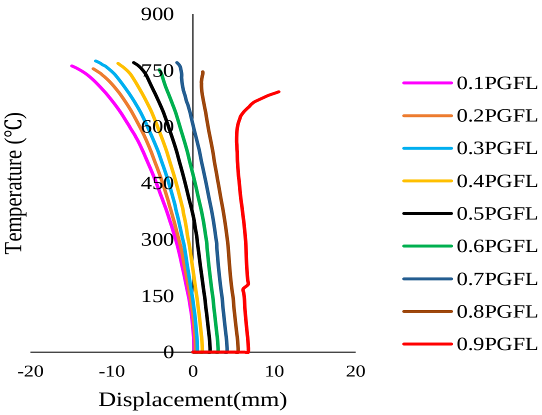

(b) Case 5

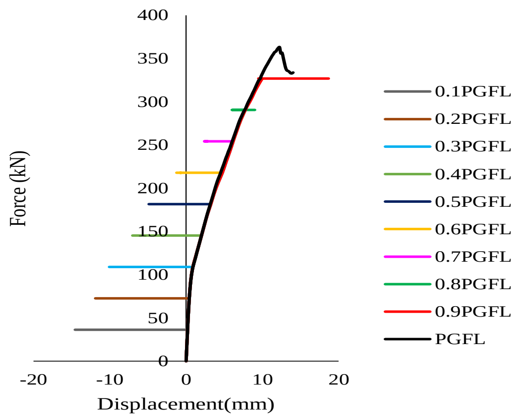

(c) Case 6

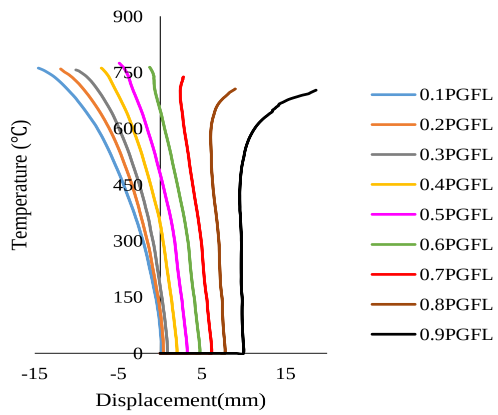

(d) Case 6

Fig. 14 Force-displacement and temperature-displacement curves

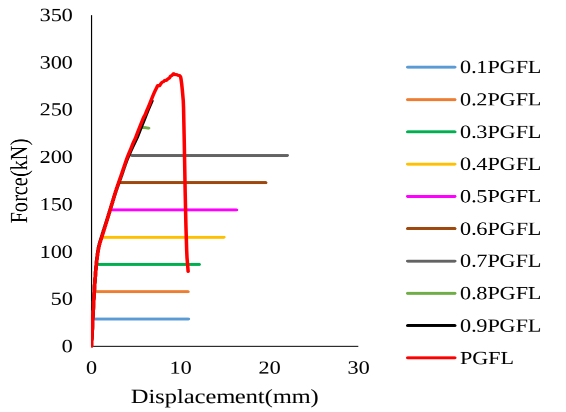

(a) Case 7

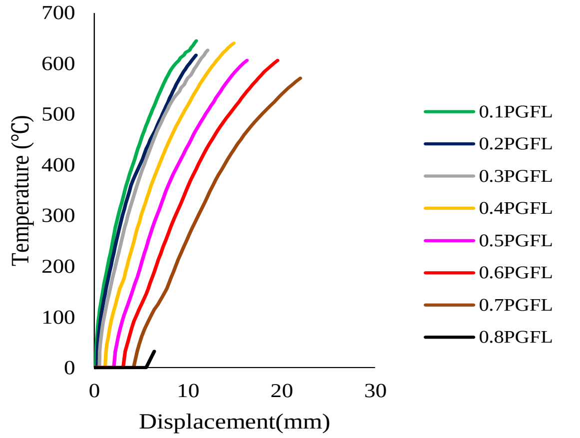

(b) Case 7

Fig. 15 Force-displacement and temperature-displacement curves

Therefore, critical crack width (ψd, ψ is the curvature of the slab and d is the effective depth of the slab) is almost the same for the specimens. Since (ψd) is almost the same for the two cases, results show that when (ψd) reaches a particular value, failure occurs. Seemingly, in temperatures corresponding to failure (600℃ or higher) modulus of elasticity degrades to 0.06 or even less of its intimal value and this parameter seems to govern the ultimate displacement and the presence of stirrup negligibly affects the critical crack width. This agrees with the findings of Annerel and Taerwe (2013).

Concerning the high-strength concrete slab case, i.e., cases 5 and 6 for which results are shown in Figs. 14(a)-(d), the failure modes and load-deflection and temperature-time trends were similar to their counterparts i.e., cases 3 and 4 and increasing the compressive strength of slab had negligible effect on the maximum temperature endured by the slab which is in agreement with the findings of Aguado *et al*. (2016). This can be justified by the fact that tensile stresses usually govern the failure mechanism in case of shear loading, cause thermal cracking and many other degradation phenomena of concrete. Tensile strength as the primary factory in punching shear was completely lost at the heated surface in all cases and the degraded modulus of elasticity in line with the thermal expansion strain and plastic strains caused the slab to undergo larger displacements in case of fire than only-static analyses as can be understood from the load-displacement graphs.

9. Conclusions

In this study punching shear of RC slabs was investigated taking into account the temperature-dependent thermal and mechanical properties of concrete and rebars. Sensitivity analyses were carried out to highlight the effect of influential parameters. The efficiency of the insulating material, gypsum was also assessed. Based on the discussions presented in previous sections, the following conclusions can be drawn:

- The numerical simulation suggests that gypsum can significantly reduce the maximum temperature transferred to the concrete; 45.8% and 70% decrease for the 10-mm and 20-mm thick gypsum, respectively.
- Increasing the flexural reinforcement ratio increases the shear capacity of the slab in fire conditions. However, the failure mode of the slab becomes brittle in most of the cases.
- Application of the fire from the top face causes the slab to deflect upwards and in an opposite direction to the gravity-load induced deflections up to the 0.7× PGFL (pure gravity failure load); this is in agreement with the key points taken by the authors from the study. For greater load levels, the deflection is in the direction of the gravity-load induced deflections.
- For the same load value, no significant differences were observed between two cases with and without shear reinforcements under fire conditions which is in agreement with key points taken by other researchers.
- For low rebar ratios, flexural punching occurred for load levels greater than 0.5×PGFL in slabs without shear reinforcement and all the load levels in slabs with shear reinforcements in the presence of fire. For high rebar ratios, however, the trend was not the same and brittle punching occurred almost in all the load levels for slabs with and without shear reinforcement under fire conditions.
- Negligible difference was observed for different compressive strengths of concrete in terms of maximum temperature endured.
- Application of fire from the bottom face, which caused additional displacements in direction of the gravity load noticeably precipitated the failure of the slab.
- Numerical analyses showed that the displacement of the slab caused by the load, thermal effects and stiffness reduction increases and the load-induced critical crack width increases due to the degradation of stiffness. The width of the so-called crack increases when the fire is applied from below and fire-induced displacements are in the direction of the load-induced displacement. However, when the fire is applied from above and it tends to deflect the slab upwards, the crack with decreases. No particularly distinct crack was observed in the top face of the slab in the vicinity of the column when the fire was applied from the top face and the initially load-induced crack was the critical crack which increased/decreased in width in the case of fire.

It should be highlighted that experimental studies on punching shear of RC slabs is very limited and further numerical and experimental studies are required with regard to punching shear of RC slabs in fire conditions with different sizes and geometries to enhance our understanding of punching shear in fire conditions and expand the few existing data concerning this issue.

References

ACI Committee 216.1-14 (2014), Guide for Determining the Fire Endurance of Concrete Elements, American Concrete Institute (ACI), Farmington Hills, Michigan.

ACI Committee 363 (2010), Report on High-Strength Concrete (ACI 363R-10), American Concrete Institute (ACI), Farmington Hills, Michigan Adetif.

Adetifa, B. and Polak, M.A. (2005), "Retrofit of slab column interior connections using shear bolts", *ACI Struct. J.*, **102**(2), 268.

Aguado, J.V., Albero, V., Espinos, A., Hospitaler, A. and Romero, M.L. (2016), "A 3D finite element model for predicting the fire behavior of hollow-core slabs", *Eng. Struct.*, **108**, 12-27.

Annerel, E., Lu, L. and Taerwe, L. (2013), "Punching shear tests on flat concrete slabs exposed to fire", *Fire Saf. J.*, **57**, pp.83-95.

Annerel, E., Taerwe, L., Merci, B., Jansen, D., Bamonte, P. and Felicetti, R. (2013), "Thermo-mechanical analysis of an underground car park structure exposed to fire", *Fire Saf. J.*, **57**, 96-106.

Arna'ot, F.H., Abid, S.R., Özakça, M. and Tayşi, N. (2017), "Review of concrete flat plate-column assemblies under fire conditions", *Fire Saf. J.*, **93**, 39-52.

Aslani, F. and Bastami, M. (2011), "Constitutive relationships for normal-and high-strength concrete at elevated temperatures", *Mater. J.*, **108**(4), 355-364.

Aslani, F., Nejadi, S. and Samali, B. (2014a), "Long-term flexural cracking control of reinforced self-compacting concrete one way slabs with and without fibres", *Comput. Concrete*, **14**(4), 419-443.

Aslani, F., Nejadi, S. and Samali, B. (2015a), "Instantaneous and time-dependent flexural cracking models of reinforced self-compacting concrete slabs with and without fibres", *Comput. Concrete*, **16**(2), 223-243

Aslani, F., Nejadi, S. and Samali, B. (2015c), "Instantaneous and time-dependent behaviour of reinforced self-compacting concrete slabs", *Concrete Aust.*, **41**(4), 52-59.

Aslani, F. and Samali, B. (2015b), "Constitutive relationships for self-compacting concrete at elevated temperatures", *Mater. Struct.*, **48**(1-2), 337-356.

Aslani, F. and Samali, B. (2014b), "Constitutive relationships for steel fibre reinforced concrete at elevated temperatures", *Fire Technol.*, **50**(5), 1249-1268.

ASTM E119-12a (2012), Standard Test Methods for Fire Tests of Building Construction and Materials, American Society for Testing and Materials (ASTM), West Conshohocken, PA.

ATENA (2016), Finite Element Software, ATENA Program Documentation, Theory and User Manual, Cervenka Consulting, Prague, Czech Republic.

Bamonte, P., Felicetti, R. and Gambarova, P.G. (2009), "Punching shear in fire-damaged reinforced concrete slabs", *ACI Spec. Publ.*, **265**, 345-366.

Bamonte, P., Fernández Ruiz, M. and Muttoni, A. (2012), "Punching shear strength of R/C slabs subjected to fire", *Proceedings of the 7th International Conference on Structures in Fire-SiF2012*, Eds. M. Fontana, A. Frangi, and M. Knobloch.

Bamonte, P. and Felicetti, R. (2009), "Fire scenario and structural behaviour of underground parking lots exposed to fire", *Appl. Struct. Fire Eng.*, Prague.

Babrauskas, V. (1993), "Structural fire protection: ASCE Manuals and Reports on Engineering Practice No. 78", Ed. T.T. Lie, American Society of Civil Engineers, New York, August.

Bažant, Z.P. and Chern, J.C. (1987), "Stress-induced thermal and shrinkage strains in concrete", *J. Eng. Mech.*, ASCE, **113**(10), 1493-1511.

Bompa, D.V. and Oneţ, T. (2016), "Punching shear strength of RC flat slabs at interior connections to columns", *Mag. Concrete Res.*, **68**(1), 24-42.

BS 8110-2 (1985), Structural Use of Concrete-Part 2: Code of Practice for Special Circumstances, British Standards Institution (BSI). London, UK.

Carette, G.G., Painter, K.E. and Malhotra, V.M. (1982), "Sustained high temperature effect on concretes made With normal portland cement, normal portland cement and slag, or normal portland cement and fly ash", *Concrete Int.*, **4**(7), 16.

Cather, B. (2003). Chapter 10: Concrete and Fire Exposure. In Advanced Concrete Technology: Concrete Properties, Vol. 2, Butterworth-Heinemann, Oxford, UK.

Cervenka, V. (2013), "Reliability-based non-linear analysis according to fib Model Code 2010", *Struct. Concrete*, **14**(1), 19-28.

Chang, Y.F., Chen, Y.H., Sheu, M.S. and Yao, G.C. (2006), "Residual stress-strain relationship for concrete after exposure to high temperatures", *Cement Concrete Res.*, **36**, 1999-2005.

Chung, J.H., Consolazio, G.R.a nd McVay, M.C. (2006), "Finite element stress analysis of a reinforced high-strength concrete column in severe fires", *Comput. Struct.*, **84**(21), 1338-1352.

Custer, R.L.P. and Meacham, B.J. (2000), *SFPE Engineering Guide to Performance Based Fire Protection Analysis and Design of Buildings*, National Fire Protection Association, Society of Fire Protection Engineers, Bethesda, MD.

Dwaikat, M.B. and Kodur, V.K.R. (2009), "Hydrothermal model for predicting fire-induced spalling in concrete structural systems", *Fire Saf. J.*, **44**(3), 425-434.

Džolev, I.M. (2018), "Numerical analysis on the behaviour of reinforced concrete frame structures in fire", *Comput. Concrete*, **21**(6), 637-647.

ElMohandes, F. (2013), "Advanced three-dimensional nonlinear analysis of reinforced concrete structures subjected to fire and extreme loads", PhD Thesis, University of Toronto, Toronto, ON, Canada.

ElMohandes, F. and Vecchio, F.J. (2016), "Reliability of temperature-dependent models for analysis of reinforced concrete members subjected to fire", *ACI Struct. J.*, **113**(3), 481.

EN 1992-1-2:2004 (2005), Eurocode 2: Design of Concrete Structures-Part 1-2: General Rules, Structural Fire Design, European Committee for Standardization (CEN), Brussels, Belgium.

Farzam, M., Fouad, N.A., Grünberg, J. and Fard, M.Y. (2010), "Punching of RC slabs under eccentric loads", *Struct. Concrete*, **11**(4), 211-220.

Farzam, M., Sadaghian, H. and Khodadade, G. (2017), "Shear behaviour of elongated rectangular wall-footing connections under eccentric loads", *Mag. Concrete Res.*, 1-36.

Fernández Ruiz, M., Muttoni, A. and Kunz, J. (2010), "Strengthening of flat slabs against punching shear using post-installed shear reinforcement", *ACI Struct. J.*, **107**(ARTICLE), 434-442.

Firmo, J.P., Arruda, M.R.T., Correia, J.R. and Tiago, C. (2015), "Flexural behaviour of partially bonded carbon fibre reinforced polymers strengthened concrete beams: Application to fire protection systems design", *Mater. Des.*, **65**, 1064-1074.

Fletcher, I.A., Welch, S., Torero, J.L., Carvel, R.O. and Usmani, A. (2007), "Behaviour of concrete structures in fire", *Therm. Sci.*, **11**(2), 37-52.

Genikomsou, A.S. and Polak, M.A. (2015), "Finite element analysis of punching shear of concrete slabs using damaged plasticity model in ABAQUS", *Eng. Struct.*, **98**, 38-48.

George, S.J. and Tian, Y. (2012), "Structural performance of reinforced concrete flat plate buildings subjected to fire", *Int. J. Concrete Struct. Mater.*, **6**(2), 111-121.

Ghoreishi, M., Bagchi, A. and Sultan, M.A. (2015), "Punching shear behavior of concrete flat slabs in elevated temperature and fire", *Adv. Struct. Eng.*, **18**(5), 659-674.

GID (2015), International Centre for Numerical Methods in Engineering (CIMNE), Barcelona, Spain.

Gosav, A.V., Kiss, Z.I., Oneţ, T. and Bompa, D.V. (2016), "Failure assessment of flat slab-to-column members", *Mag. Concrete Res.*, **68**(17), 887-901.

Harmathy, T.Z. (1970), "Thermal properties of concrete at elevated temperatures", *Am. Soc. Test. Mater. J. Mater.*, **5**(1), 47-74.

Hertz, K.D. (1980), "Betonkonstruktioners brandtekniske egenskaber (Fire properties of concrete constructions) - Part 1 - BYG Rapport No. R-141", PhD Thesis, Technical University of Denmark (DTU), Lyngby, Denmark.

Hertz, K.D. (2005), "Concrete strength for fire safety design", *Mag. Concrete Res.*, **57**(8), 445-453.

Hertz, K.D. (2003), "Limits of spalling of fire-exposed concrete", *Fire Saf. J.*, **38**(2), 103-116.

Hwang, J.W., Ha, S.H., Lee, Y.H., Kim, W.J. and Kwak, H.G. (2013), "A numerical model to evaluate fire-resistant capacity of the reinforced concrete members", *J. Korea Concrete Inst.*, **25**(5), 497-508.

Hwang, J.Y. and Kwak, H.G. (2015), "A mumerical ,odel of reinforced concrete members exposed to fire and after-cooling analysis", *J. Comput. Struct. Eng. Inst. Korea*, **28**(1), 101-113.

Ibrahimbegovic, A., Boulkertous, A., Davenne, L., Muhasilovic, M. and Pokrklic, A. (2010), "On modeling of fire resistance tests on concrete and reinforced-concrete structures", *Comput. Concrete*, **7**(4), 285-301.

ISO 834-1 (1999), Fire-Resistance Tests-Elements of Building Construction-Part 1: General Requirements, International Organization for Standardization (ISO), Geneva, Switzerland.

Jadooe, A., Al-Mahaidi, R. and Abdouka, K. (2017), "Experimental and numerical study of strengthening of heat-damaged RC beams using NSM CFRP strips", *Constr. Build. Mater.*, **154**, 899-913.

Kodur, V.K.R., Wang, T.C. and Cheng, F.P. (2004), "Predicting the fire resistance behaviour of high strength concrete columns", *Cement Concrete Compos.*, **26**(2), 141-153

Kodur, V.K.R. and Dwaikat, M. (2008), "A numerical model for predicting the fire resistance of reinforced concrete beams", *Cement Concrete Compos.*, **30**(5), 431-443.

Kodur, V.K.R. and Phan, L. (2007), "Critical factors governing the fire performance of high strength concrete systems", *Fire Saf. J.*, **42**(6-7), 482-488.

Kontogeorgos, D.A., Mandilaras, I.D. and Founti, M.A. (2015), "Fire behavior of regular and latent heat storage gypsum boards", *Fire Mater.*, **39**(5), 507-517.

Kordina, K. (1997), Über das Brandverhalten Punktgestützter Stahlbetonplatten, (No. 479.

Kotsovos, G.M. and Kotsovos, M.D. (2010), "A new approach to designing reinforcement to resist punching shear", *Struct. Eng.*, **88**(8), 20-25.

Kotsovos, M.D. (2014), *Design for Punching of Flat Slabs*, Compressive Force-Path Method, Springer, Cham.

Li, L. and Purkiss, J.A. (2005), "Stress-strain constitutive equations of concrete material at elevated temperatures", *Fire Saf. J.*, **40**, 669-686.

Liao, J.S., Cheng, F.P. and Chen, C.C. (2013), "Fire resistance of concrete slabs in punching shear", *J. Struct. Eng.*, **140**(1), 04013025.

Malhotra, H.L. (1982), *Design of Fire-Resisting Structures*, Surrey University Press, London, UK.

Moss, P.J., Dhakal, R.P., Wang, G. and Buchanan, A.H. (2008), "The fire behaviour of multi-bay, two-way reinforced concrete slabs", *Eng. Struct.*, **30**(12), 3566-3573.

Naus, D.J. (2010), "A compilation of elevated temperature concrete material property data and information for use in assessments of nuclear power plant reinforced concrete structures (NUREG/CR-7031)", United States Nuclear Regulatory Commission (U.S.NRC), Office of Nuclear Regulatory Research, Oak Ridge, TN.

Brushlinsky, N.N., Hall, J.R., Sokolov, S.V. and Sokolov, P. (2015), "World fire statistics, centre of fire statistics of CTIF", *International Association of Fire and Rescue Services*, No. 20.

Ožbolt, J., Bošnjak, J., Periškić, G. and Sharma, A. (2014), "3D numerical analysis of reinforced concrete beams exposed to elevated temperature", *Eng. Struct.*, **58**, 166-174.

Petzold, A. and Röhrs, M. (1970), *Concrete for High Temperatures*, Eds. Phillips, A.B. and Turner, F.H., 2 Edition, McLaren and Sons, London.

Phan, L.T. (1996), "Fire performance of high-strength concrete: A report of the stateof-the-art, NISTIR 5934", Building and Fire Research Laboratory, National Institute of Standards and Technology (NIST), Gaithersburg, MD.

Rahmanian, I. and Wang, Y.C. (2012), "A combined experimental and numerical method for extracting temperature-dependent thermal conductivity of gypsum boards", *Constr. Build. Mater.*, ***26***(1), 707-722.

Salem, H., Issa, H., Gheith, H. and Farahat, A. (2012), "Punching shear strength of reinforced concrete flat slabs subjected to fire on their tension sides", *HBRC J.*, **8**(1), 36-46.

Smith, H., Stratford, T. and Bisby, L. (2016), "Deflection response of reinforced concrete slabs tested in punching shear in fire", *Appl. Struct. Fire Eng.*, DOI: https://doi.org/10.14311/asfe.2015.031

Song, Y., Zhang, Z., Qing, L. and Yu, C. (2007), "Biaxial tensile-compressive experiment of concrete at high temperatures", *Front. Arch. Civil Eng. China*, **1**(1), 94-98.

Wang, Y., Burgess, I., Wald, F. and Gillie, M. (2012), *Performance-based Fire Engineering of Structures*, CRC Press.

Wijayasinghe, M. (2011), "Fire losses in Canada year 2007 and selected years", Council of Canadian Fire Marshals and Fire Commissioners, Calgary, Alberta, Canada.

Wosatko, A., Pamin, J., Winnicki, A., Putanowicz, R. and Polak, M.A. (2006), "Numerical simulation of damage in reinforced concrete slab-column connection", *Proc. EURO-C 2006 Int. Conf. Computational Modelling of Concrete Structures*, 881-889.

CC

Appendix A

Table A1 Compressive strength of concrete at elevated temperatures

References	Compressive strength at elevated temperatures
Bažant and Chern (1987)	$f'_{cT} = f'_c(1 - 0.1786 \times 10^{-3}T) \quad T \le 350℃;$ $f'_{cT} = f'_c(0.9375 - 1.713 \times 10^{-3}(T - 350) \;\; 350℃ \le T \le 800℃$
ASCE (1993)	$f'_{cT} = f'_c \quad 20℃ \le T \le 450℃; \;\; f'_{cT} = f'_c\left[2.011 - 2.353\left(\frac{T-20}{1000}\right)\right]$ $450℃ \le T \le 874℃; \;\; f'_{cT} = 0 \;\; T > 874℃$
Kodur *et al*. (2004)	$f'_{cT} = \begin{Bmatrix} f'_c[1 - 0.003125(T-20)] & T \le 700℃ \\ 0.75f'_c & 100° \le T \le 400℃ \\ f'_c[1.33 - 0.00145T] & T > 400℃ \end{Bmatrix}$
Li and Purkiss (2005)	$f'_{cT} = f'_c \;\; (0.00165\left(\frac{T}{100}\right)^3 - 0.03\left(\frac{T}{100}\right)^2 + 0.025\left(\frac{T}{100}\right) + 1.002)$
Hertz (2005)	$f'_{cT} = f'_c[1/(1 + \frac{T}{T_1} + \left(\frac{T}{T_2}\right)^2 + (\left(\frac{T}{T_8}\right)^8 + \left(\left(\frac{T}{T_{64}}\right)^{64}\right)]$ Siliceous aggregate: $T_1 = 15000, T_2 = 800, T_8 = 800, \; T_{64} = 100000$ Lightweight aggregate: $T_1 = 100000, \; T_2 = 1100, \; T_8 = 800, \; T_{64} = 940$ Other aggregates: $T_1 = 100000, \; T_2 = 1080, \; T_8 = 690, \; T_{64} = 1000$
Aslani and Bastami (2011)	$f'_{cT} = f'_c\begin{bmatrix} 1.01 - 0.0006T \le 1.0 & 20℃ \le T \le 200℃ \\ 1.0565 + 0.0017T + 5 \times 10^{-6}T^2 - 5 \times 10^{-9}T^3 & 200℃ < T \le 900℃ \\ 0 & T > 900℃ \end{bmatrix}$ Calcareous aggregate

Note: f'_{cT}: Compressive of concrete at elevated temperatures

Table A2 Tensile strength of concrete at elevated temperatures

References	Tensile strength at elevated temperatures
Bažant and Chern (1987)	$f'_{tT} = f'_t\begin{Bmatrix} 1.010052 - 0.526 \times 10^{-3}T & T \le 400℃ \\ 1.08 - 2.5 \times 10^{-3}T & 400℃ < T \le 600℃ \\ 0.6 - 0.5 \times 10^{-3}T & 600℃ < T \le 1200℃ \end{Bmatrix}$
EC2 (BS EN1992-1-2:2004)	$f'_{tT} = f'_t\begin{Bmatrix} 1 & T \le 100℃ \\ 1 - \frac{T-100}{500} & 100℃ < T \le 600℃ \end{Bmatrix}$
Chang *et al*. (2006)	$f'_{tT} = f'_t\begin{Bmatrix} 1.05 - 2.5 \times 10^{-3}T & 20℃ \le T \le 100℃ \\ 0.8 & 100℃ < T \le 200℃ \\ 1.02 - 1.1 \times 10^{-3}T \;\; \ge 0.0 & 200℃ < T \le 800℃ \end{Bmatrix}$
Song *et al*. (2007)	$f'_{tT} = f'_t(0.9798 - 0.001T); \quad T \le 979.8℃$
Aslani and Bastami (2011)	$f'_{tT} = f'_t\begin{Bmatrix} 1.02 - 9.8 \times 10^{-4}T \le 1.0 & 20℃ \le T \le 100℃ \\ 0.965 - 1 \times 10^{-4}T - 9 \times 10^{-7}T^2 - 3 \times 10^{-9}T^3 + 3.2 \times 10^{-12}T^4 & 100℃ < T \le 200℃ \\ 0 & 200℃ < T \le 800℃ \end{Bmatrix}$

Table A3 Modulus of elasticity of concrete at elevated temperatures

References	Modulus of elasticity at elevated temperatures
Bažant and Chern (1987)	$E_{cT} = E_c\begin{Bmatrix} 1 - 1.256 \times 10^{-3}T & T \le 650℃ \\ -0.565 \times 10^{-3}(T - 650) + 0.1837 & 650℃ < T \le 800℃ \end{Bmatrix}$
Li and Purkiss (2005)	$E_{cT} = E_c\begin{Bmatrix} 1 & T \le 60℃ \\ \frac{800-T}{740} & 60℃ < T \le 800℃ \end{Bmatrix}$
Chang *et al*. (2006)	$E_{cT} = E_c\begin{Bmatrix} 1.33 - 1.65 \times 10^{-3}T & 20℃ \le T \le 100℃ \\ 0.8 & 100℃ < T \le 200℃ \\ 1.02 - 1.1 \times 10^{-3}T \;\; \ge 0.0 & 200℃ < T \le 800℃ \end{Bmatrix}$
Aslani and Bastami (2011)	$E_{cT} = E_c\begin{Bmatrix} 1 & 20℃ \le T \le 100℃ \\ 1.015 - 0.00154T + 2 \times 10^{-7}T^2 + 3 \times 10^{-10}T^3 & 100℃ < T \le 1000℃ \\ 0 & 1000℃ < T \end{Bmatrix}$

Note: E_c: Modulus of elasticity of concrete at ambient temperatures; E_{cT}: Modulus of elasticity of concrete at elevated temperatures.

Table A4 Values for main parameters of normal-strength and high-strength concrete at elevated temperatures (BS EN1992-1-2:2004)

Temperature, ℃	Normal-strength concrete						High-strength concrete		
	Siliceous aggregate			*Calcareous aggregate*			$f'_{cT}/f'_c(20℃)$		
	$f'_{cT}/f'_c(20℃)$	$\varepsilon_{c1,T}$	$\varepsilon_{cu1,T}$	$f'_{cT}/f'_c(20℃)$	$\varepsilon_{c1,T}$	$\varepsilon_{cu1,T}$	Class 1	Class 2	Class 3
20	1	0.0025	0.02	1	0.0025	0.02	1	1	1
100	1	0.004	0.0225	1	0.004	0.023	0.9	0.75	0.75
200	0.95	0.0055	0.025	0.97	0.0055	0.025	0.9	0.75	0.7
300	0.85	0.007	0.0275	0.91	0.007	0.028	0.85	0.75	0.65
400	0.75	0.01	0.03	0.85	0.01	0.03	0.75	0.75	0.45
500	0.6	0.015	0.0325	0.74	0.015	0.033	0.6	0.6	0.3
600	0.45	0.025	0.035	0.6	0.025	0.035	0.45	0.45	0.25
700	0.3	0.025	0.0375	0.43	0.025	0.038	0.3	0.3	0.2
800	0.15	0.025	0.04	0.27	0.025	0.04	0.15	0.15	0.15
900	0.08	0.025	0.0425	0.15	0.025	0.043	0.08	0.113	0.08
1000	0.04	0.025	0.045	0.06	0.025	0.045	0.04	0.075	0.04
1100	0.01	0.025	0.0475	0.02	0.025	0.048	0.01	0.038	0.01
1200	0	---	---	0	---	---	0	0	0

Notes: High-strength concrete is classified into three categories depending on its compressive strength according to EC2 (BS EN1992-1- 2:2004).
* Class 1 for compressive strengths between C50/67 and C60/75;
* Class 2 for compressive strengths between C70/85 and C80/95;
* Class 3 for compressive strengths greater than C90/150.
* The symbol Ca/b denotes a concrete with a characteristic compressive strength of "a" MPa and cubic compressive strength of "b" MPa, respectively.
* In cases where the actual charasteristic compressive strength is higher than those specified in the design, relative reduction factor of the higher class should be used for fire design.

Table A5 Constitutive relationships for temperature-dependent properties of concrete

	ASCE (1993) (NSC)	EC2 (BS EN1992-1-2:2004)
Stress- strain relationships	$\sigma_c = \begin{cases} f'_{cT}[1-\left(\frac{\varepsilon-\varepsilon_{max,T}}{\varepsilon_{max,T}}\right)^2, \varepsilon \le \varepsilon_{max,T} \\ f'_{cT}[1-\left(\frac{\varepsilon_{max,T}-\varepsilon}{3\varepsilon_{max,T}}\right)^2, \varepsilon > \varepsilon_{max,T} \end{cases}$ $f'_{cT} = \begin{cases} f'_c & 20^\circ\text{C} \le T \le 450^\circ\text{C} \\ f'_c[2.011-2.353\left(\frac{T-20}{1000}\right)] & 450^\circ\text{C} \le T \le 874^\circ\text{C} \\ 0 & T > 874^\circ\text{C} \end{cases}$ $\varepsilon_{max,T} = 0.025 + (6.0T + 0.04T^2) \times 10^{-6}$	$\sigma_c = \frac{3\varepsilon f'_{cT}}{\varepsilon_{c1,T}(2+\left(\frac{\varepsilon}{\varepsilon_{c1,T}}\right)^3)}, \varepsilon \le \varepsilon_{cu1,T}$ Nonlinear descending branch is permitted for $\varepsilon_{c1,T} < \varepsilon \le \varepsilon_{cu1,T}$ instead of the linear branch in the numerical analysis.
	Siliceous aggregate concrete	*Specific heat (J/kg°C)*
	$\rho c = \begin{cases} 0.005T + 1.7 & 20^\circ\text{C} \le T \le 200^\circ\text{C} \\ 2.7 & 200^\circ\text{C} < T \le 400^\circ\text{C} \\ 0.013 - 2.5 & 400^\circ\text{C} < T \le 500^\circ\text{C} \\ 10.5 - 0.013T & 500^\circ\text{C} < T \le 600^\circ\text{C} \\ 2.7 & 600^\circ\text{C} < T \end{cases}$	$c = 900 \quad 20^\circ\text{C} \le T \le 100^\circ\text{C}$ $c = 900 + (T-100) \quad 100^\circ\text{C} \le T \le 200^\circ\text{C}$ $c = 900 + (T-200)/2 \quad 200^\circ\text{C} \le T \le 400^\circ\text{C}$ $c = 1100 \quad 400^\circ\text{C} \le T \le 1200^\circ\text{C}$
Thermal capacity	*Calcareous aggregate concrete*	*Density change (kg/m³)*
	$\rho c = \begin{cases} 2.566 & 20^\circ\text{C} \le T \le 400^\circ\text{C} \\ 0.1765T - 68.034 & 400^\circ\text{C} < T \le 410^\circ\text{C} \\ 25.00671 - 0.05043T & 410^\circ\text{C} < T \le 445^\circ\text{C} \\ 2.566 & 445^\circ\text{C} < T \le 500^\circ\text{C} \\ 0.01603T - 5.44881 & 500^\circ\text{C} < T \le 635^\circ\text{C} \\ 0.16635T - 100.90225 & 635^\circ\text{C} < T \le 715^\circ\text{C} \\ 176.07343 - 0.22130T & 715^\circ\text{C} < T \le 785^\circ\text{C} \\ 2.566 & 785^\circ\text{C} < T \end{cases}$	$\rho = \rho(20^\circ\text{C}) = reference\ density$ $20^\circ\text{C} \le T \le 115^\circ\text{C}$ $\rho = \rho(20^\circ\text{C})(1 - \frac{0.02(T-115)}{85})$ $100^\circ\text{C} \le T \le 200^\circ\text{C}$ $\rho = \rho(20^\circ\text{C})(0.98 - \frac{0.03(T-200)}{200})$ $200^\circ\text{C} \le T \le 400^\circ\text{C}$ $\rho = \rho(20^\circ\text{C})(0.95 - \frac{0.07(T-400)}{800})$ $400^\circ\text{C} \le T \le 1200^\circ\text{C}$
Thermal conductivity	*Siliceous aggregate concrete* $k_c = \begin{cases} -0.000625T + 1.5 & 20^\circ\text{C} \le T \le 800^\circ\text{C} \\ 1 & 800^\circ\text{C} < T \end{cases}$ *Calcareous aggregate concrete* $k_c = \begin{cases} 1.355 & 20^\circ\text{C} \le T \le 293^\circ\text{C} \\ -0.001241T + 1.7162 & 293^\circ\text{C} < T \end{cases}$	All types *Upper limit* $k_c = 2 - 0.2451\left(\frac{T}{100}\right) + 0.0107\left(\frac{T}{100}\right)^2$ $20^\circ\text{C} \le T \le 1200^\circ\text{C}$ *Lower limit* $k_c = 1.36 - 136\left(\frac{T}{100}\right) + 0.0057\left(\frac{T}{100}\right)^2$ $0^\circ\text{C} \le T \le 1200^\circ\text{C}$
Thermal strain	All types: $\varepsilon_{th} = [0.004(T^2 - 400) + 6(T-20)] \times 10^{-6}$	*Siliceous aggregate concrete* $\varepsilon_{th} = -1.8 \times 10^{-4} + 9 \times 10^{-6}T + 2.3 \times 10^{-11}T^3$ $20^\circ\text{C} \le T \le 700$ $\varepsilon_{th} = 14 \times 10^{-3} \quad 20^\circ\text{C} \le T \le 1200^\circ\text{C}$ *Calcareous aggregate* $\varepsilon_{th} = 1.2 \times 10^{-4} + 6 \times 10^{-6}T + 1.4 \times 10^{-11}T^3$ $20^\circ\text{C} \le T \le 805^\circ\text{C}$ $\varepsilon_{th} = 12 \times 10^{-3} \quad 805 < T \le 1200^\circ\text{C}$

σ_c: Stress of concrete; ε: Concrete mechanical strain; $\varepsilon_{c1,T}$: Concrete strain at maximum stress at temperature T; $\varepsilon_{cu1,T}$: Concrete ultimate strain at temperature T; ε_{max}: Concrete strain at maximum stress at temperature T; c: Concrete specific heat (J/kg°C) $\rho(T)$: Density of concrete at temperature T, kg/m^3 ; $\rho(20^\circ\text{C})$: Density of concrete at room temperature T, kg/m^3.